UNDERSEA & HYPERBARIC MEDICINE

# Post-decompression bubble and inflammation interactions: a non-extensive dynamical system model

**Sérgio Rhein Schirato [1], Vitor Silva [1], Kátia Iadocicco [1], Alessandro Marroni [2], Massimo Pieri [2], Danilo Cialoni [2,3], José Guilherme Chaui-Berlinck [1]**

[1] Department of Physiology, Biosciences Institute, University of São Paulo

[2] DAN Europe Research Division, Roseto degli Abruzzi, Italy

[3] Environmental Physiology and Medicine Laboratory, Department of Biomedical Sciences, University of Padova, Padova, Italy

**CORRESPONDENCE:** Sergio Rhein Schirato – *sergio.schirato@daemoninvestments.com*

## ABSTRACT

**Schirato SR, Silva V, Iadocicco K, et al. Post-decompression bubble and inflammation interactions: a non-extensive dynamical system model. Undersea Hyperb Med. 2022 Second Quarter; 49(2) 207-226.**

Inert gas bubbles in tissues and in blood have been historically considered as the only triggering factors for DCS, but now many other factors are considered to affect the final outcome of a decompression profile for a certain individual. In this sense, inflammation seems to play a relevant role, not only due to the physical damage of tissues by the bubbles, but as a potentiator of the process as a whole. The present study aims to put forward a mathematical model of bubble formation associated with an inflammatory process related to decompression. The model comprises four state-variables (inert gas pressure, inert gas bubbles, proinflammatory and inflammatory factors) in a set of non-linear differential equations. The model is non-extensive: inert gas transitions between liquid and gaseous phases do not change the concentration of the dissolved gas. The relationship between bubbles and inflammation is given through parameters that form a positive feedback loop. The results of the model were compared with the experimental results of echocardiography from volunteers in two dive/decompression profiles; the model shows a very good agreement with the empirical data and previews different inflammatory outcomes for different experimental profiles. We suggest that slight changes in the parameters' values might turn the simulations from a non-inflammatory to an inflammatory profile for a given individual. Therefore, the present model might help address the problem of DCS on a particular basis.

**KEYWORDS:** bubble formation; decompression sickness; dynamical system; inert gas pressure

## 1. INTRODUCTION

Subjects exposed to hyperbaric environments and subsequent decompression might develop what has become known as decompression sickness, or simply, DCS. DCS is a disease that manifests itself through a variety of symptoms ranging from innocuous joint or skeletal pain, to neurological impairment, and even death. Since the first study published by the Haldane group [1] at the beginning of the 20th century, different algorithms have been developed to create safe decompression profiles, or at least to keep the incidence of DCS limited to a predetermined expected limit.

Decompression sickness has historically been associated with the formation of bubbles, and this understanding is still very much accepted. For instance, a series of three articles recently published correlate symptoms of DCS to tissue perfusion alterations that, ultimately, cause the pressure of inert gas to rise enough to produce bubbles in a specific location [2-4]. Due to the clear causal relationship embedded in this physical explanation, mathematical modeling has been employed extensively to address the formation of bubbles and their fate during dive/decompression procedures.

As a few examples, Lewis [5] developed a non-extensive model (see section 3) that incorporates ambient pressure, tissue inert gas pressure, depth and a safety factor of the ratio between tissue to ambient pressure. The author tries to determine the safe rate of ascent based on these variables. Van Liew and Burkard [6] present modeling in which bubbles surrounding tissue and blood perfusion are taken into account in the inert gas dynamics. Their model is extensive, and depletion of nitrogen due to bubble formation dampens out further increase either in numbers or in sizes. They conclude that such a competition for the inert gas among those three compartments would render the removal of inert gas a linear function of time after emersion.

The physical growth of the bubbles is another relevant topic also pursued in modeling. For instance, the role of nucleating hydrophobic pockets was explored by Chappell and Payne [7] in a model that takes into account surface tension and metabolic gases besides the inert one. Even though the authors discuss the formation/growth of bubbles, they do not present a putative time-profile of bubbles that could be found in the bloodstream. The same applies to the other two models just cited.

On the other hand, Gutvik and Brubakk [8] developed an extensive model that tries to simulate the venous gas emboli time-profile as detected by echo-Doppler. Bubble growth and dislodgement (i.e., migration to venous blood) are modeled as physical and probabilistic events, respectively. Their simulated results seem to be in good agreement with empirical data (Figure 4). They conclude that improvements to the model might help in DCS risk assessment.

In a review of both the models and the physical/physiological assumptions behind bubble formation and of DCS, Papadopoulou and colleagues [9] conclude that: "In any case, incorporating bubble formation and growth mechanisms in decompression models is important and the general direction of research in that area is an effort to make models more biophysical to allow better extrapolation." In this vein, Arieli and Marmur [10] analyze a model based on active hydrophobic spots to relate bubble presence along the arterial tree. The model is related to their experimental data of ex-vivo heart-lung preparations from sheep. They define individuals as "bubblers" or "non-bubblers" in relation to unknown physiological variables that would enhance the probability of bubble formation/detachment to cause DCS, and they try to obtain the probabilities of DCS given the formation of bubbles.

Even though DCS seems to have a correlation with inert gas bubbles in blood and tissues, since the use of ultrasound technology to access decompression stress it became clear that even mild exposures to hyperbaric environments and subsequent decompression would lead to bubble formation in the venous circulation [11]. Therefore, the relationship between the observed venous gas emboli and DCS becomes weak, and bubbles detected by two-dimensional echocardiography are a poor surrogate for DCS [12]. In fact, there is a large interindividual variance in the post-decompression venous gas emboli production [12,13]; high bubble grades (according to the Eftedal-Brubakk (EB) scale, see below) are observed frequently in individuals without symptoms of DCS. On the other hand, while this seems to be true on an individual basis, in a large enough sample higher grades of venous gas emboli are expected to be associated with higher probability of DCS symptoms development [14,15].

If physical factors alone, such as hydrostatic pressure variation, nucleation, surface tension and tissue inert gas capacitance, were the sole factors to trigger bubble formation and, eventually, DCS, then similar bubble production for individuals with similar body composition exposed to similar compression-decompression profiles should be expected – something that is not observed [16].

One study has shown that exposure to high-pressure environments – even in the absence of decompression – is sufficient to increase the production of microparticles (MPs) that carry

interleukin-1-beta (IL-1β) [17], an important mediator in inflammatory responses. The same study demonstrated that individuals exposed to higher ambient pressures produced a higher average count of MPs after the dive, which persisted for at least two hours, while the changes observed in the group exposed to lower ambient pressures resolved within two hours after the dive. Other studies demonstrated that the compression-decompression process is related not only to increased number of MPs, but also to increased production of myeloperoxidase, an enzyme linked to the production of reactive oxygen species through nicotinamide adenine dinucleotide phosphate hydrogen (NADPH) oxidase and increased neutrophil activation [18,19]. Decreases in platelet counts, probably due to their activation and aggregation, have been observed in at least one study [20], while another study has demonstrated that such reduction could be used as a predictor of severity of the DCS symptoms in rats [21]. Based on the above, it seems reasonable to assume that DCS is not only a consequence of mechanical damage caused by bubbles, but also results from a complex biochemical process in which inflammation seems to be a relevant component. In a similar way as the "bubblers/non-bubblers" of Arieli and Marmur [10], there might be "flamers/extinguishers," where the individual DCS outcome is somehow related to the individual susceptibility to develop inflammatory processes when exposed to hyperbaric environments.

The aim of the present study is to develop a mathematical model that incorporates the physical aspects of local and venous inert gas bubble formation combined with a simplified inflammatory process triggered by, and also possibly potentiating, these bubbles. Results are then compared to empirical echocardiography data from our group.

## 2. MATERIALS AND METHODS

### 2.1. Subjects

A total of 20 divers (19 male and one female) participated in this study. No symptoms of DCS were observed during the experimental dives.

**Table 1. Study population characteristics**

| VARIABLE | MEAN | SD |
|---|---|---|
| age (years) | 42.78 | 5.79 |
| weight (kg) | 86.55 | 14.47 |
| height (cm) | 179.63 | 6.66 |
| BMI | 26.90 | 4.78 |

BMI – body mass index; SD – standard deviation

Table 1 summarizes the anthropometric data of the study population.

The present study was undertaken in healthy individuals, all trained divers experienced in the experimental profiles utilized. All divers provided a written informed consent. The experiments were approved by the Ethical Committee of the Università degli Studi di Milano, Italy (Aut. No. 37/17).

### 2.2. Experimental protocol

#### 2.2.1. Dives and decompression profiles

The dives were undertaken at the Y – 40 Swimming Pool, located at Montegrotto Terme, PD, Italy. All volunteers used self-contained breathing apparatus (scuba). The breathing gases consisted of a mix of 21% oxygen, 35% helium and 44% nitrogen at a pressure of 528 kPa (42 meters of seawater) for a bottom time of 40 minutes. Divers descended at a rate of approximately 20 msw/minute, reaching the bottom of the water column in approximately two minutes. Subjects were decompressed at a rate of 9 msw/minute until the first decompression stop. At a pressure of 324 KPa (21 msw) the breathing gas was changed to 50% oxygen and 50% nitrogen. Dive profiles are detailed in Table 2.

The volunteers undertook two different decompression profiles, with an interval of 48 hours between dives. One profile was determined through the application of Bühlmann's ZHL16-C algorithm without any modification [22]. This profile will be referred as ZHL. The original limits in Bühlmann's algorithm are given computing the maximal pressure for a given compartment ***j*** as:

$$P_{max\,j} = \frac{P_{amb}}{bj} + a_j \qquad (1)$$

From equation (1), the second profile had supersaturation pressures for each compartment at the

**Table 2. Experimental dive profiles**

| ADJUSTED ZHL PROFILE | | | ZHL PROFILE | | |
|---|---|---|---|---|---|
| depth (msw) | time (minutes) | breathing gas composition | depth (msw) | time (minutes) | breathing gas composition |
| 42 | 40 | 21% $O_2$ / 35% He / 44% $N_2$ | 42 | 40 | 21% $O_2$ / 35% He / 44% $N_2$ |
| 21 | 4 | 50% $O_2$ / 50% $N_2$ | 9 | 4 | 50% $O_2$ / 50% $N_2$ |
| 18 | 3 | 50% $O_2$ / 50% $N_2$ | 6 | 27 | 50% $O_2$ / 50% $N_2$ |
| 15 | 3 | 50% $O_2$ / 50% $N_2$ | | | |
| 12 | 3 | 50% $O_2$ / 50% $N_2$ | | | |
| 9 | 9 | 50% $O_2$ / 50% $N_2$ | | | |
| 6 | 14 | 50% $O_2$ / 50% $N_2$ | | | |
| 3 | 5 | 50% $O_2$ / 50% $N_2$ | | | |

end of the experiment adjusted so that: $a_{j,adjusted} = 0.85\ a_j$ and factor $b_j$ was adjusted to calculate stops at 0.20 of the original pressure limits given by Bühlmann's values. This profile will be referred to as Adjusted ZHL.

A third profile, described by Schirato et al. [23] will be defined arbitrarily as "Standard" and is detailed in Table 3 for reference.

**Table 3. Standard dive profile**

| depth (msw) | time (minutes) | breathing gas composition |
|---|---|---|
| 45 | 30 | 21% $O_2$ / 35% He / 44% $N_2$ |
| 21 | 1 | 50% $O_2$ / 50% $N_2$ |
| 18 | 1 | 50% $O_2$ / 50% $N_2$ |
| 15 | 2 | 50% $O_2$ / 50% $N_2$ |
| 12 | 3 | 50% $O_2$ / 50% $N_2$ |
| 9 | 5 | 50% $O_2$ / 50% $N_2$ |
| 6 | 26 | 100% $O_2$ |

### 2.2.2. Echocardiography

Echocardiography recordings were taken every 15 minutes starting from the moment when divers left the water until 90 minutes after the dive was over. Measurements were made at the Y–40 facilities using a commercially available instrument (Esaote MyLab Five SN 05-02864) and following standard procedures of this technique. Result are from observations in subjects in resting conditions. Bubbles were graded according to the EB scale and with the consensus guideline of ultrasound use in diving research [24] (Table 4).

**Table 4. Echocardiographic EB scale of bubble grading**

| GRADE | OBSERVABLE |
|---|---|
| 0 | no bubbles |
| 1 | occasional bubbles |
| 2 | at least one bubble per 4 heart cycles |
| 3 | at least one bubble per cycle |
| 4 | continuous bubbling |
| 5 | "white out" - impossible to identify individual bubbles |

## 3. MODEL

As it was advanced in the Introduction, the model is intended to combine the physical presence of bubbles with the triggering of an inflammatory process. Inflammation is a process that might, once a certain threshold is attained, become self-sustained. This is very important because even in the absence of the initial stimulus, the inflammatory process can then go forward on its own. On the other hand, decrease of the initial stimulus will dampen out its continuity when the system is below that threshold.

The model is non-extensive. This means that the transfer of inert gas between the dissolved phase in organic fluids and the gas phase in bubbles does not alter the partial pressure of the inert gas in the liquid phase. Such an assumption implies that bubble formation is not limited by the amount of inert gas present, and the quantity of bubbles in the compartments is given by the rates of formation and washout (see below).

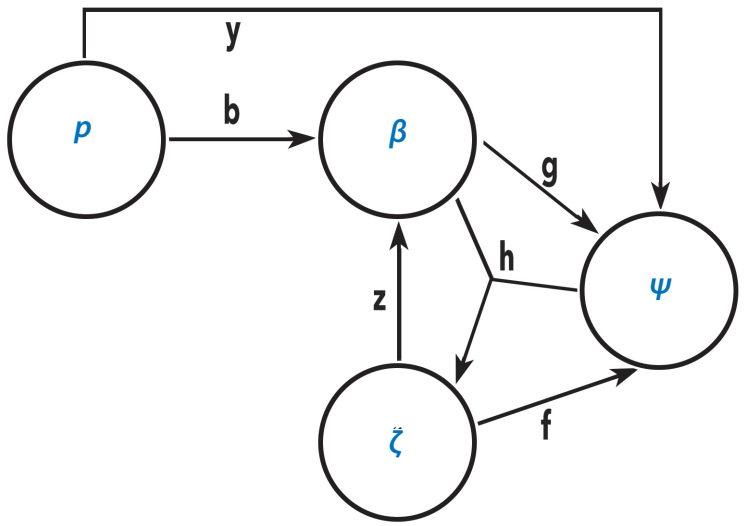


**Figure 1.**
Schematic representation of the dynamical system model for one given organic compartment.

State variables are:
***p*** - inert gas pressure;
***β*** - bubbles;
***Ψ*** and ***ζ*** - inflammatory components.

The arrows point to the influence of one state-variable over the others through the indicate rate-constants next to them.

Each state-variable has its respective washout (not represented in the figure). See text for details.

The events modeled in a given organic compartment ***j*** are described next. The formation of bubbles (***β***) is initially triggered by the nitrogen pressure (***p***) rising above the ambient pressure. This bubble formation causes the rise of a proinflammatory factor (***Ψ***). Depending on the supersaturation capacity of the tissue (herein simply referred to as maximum values or M-values), this proinflammatory factor ***Ψ*** is also stimulated by the inert gas pressure. This aims to represent how a particular tissue might or might not be susceptible to the impairment caused by the rising of inert gas pressure. Then, the simultaneous presence of bubbles and proinflammatory factor stimulates an inflammatory factor (***ζ***). The inflammatory factor ***ζ*** in turn functions as a further nucleation site for bubble formation and also stimulates further release of factor ***Ψ***. This interaction among ***β***, ***ζ*** and ***Ψ*** gives two important features to the model: (1) it is a self-sustained process; and (2) it can be alleviated by a recompression, i.e., taking the individual back to hyperbaric environment. Note that ***Ψ*** and ***ζ*** are lumped variables corresponding to sets of biological entities that play proinflammatory and inflammatory roles. Figure 1 illustrates the state variables of the model and their relationships in a given organic compartment. Numerical simulations (integrations) were performed in R version 3.6.3 ( *www.r-project.org* ) and in SimuLink, Matlab R15a (The MathWorks Inc.).

The dynamical system for a given compartment ***j*** is then given by four differential equations:

$$\dot{p}_j = \frac{Q_j}{V_j}\frac{B_s}{B_j}(P_A - p_j) \quad (2a)$$

$$\dot{\beta}_j = (p_j - P_B)\cdot(b + \bar{\delta}\cdot z\cdot\zeta_j) - m_\beta\cdot\frac{Q_j}{V_j}\cdot\beta_j \quad (2b)$$

$$\dot{\psi}_j = (p_j - M_{val,j})\cdot\bar{\delta}\cdot y + f\cdot\zeta_j + g\cdot\beta_j - m_\psi\cdot\psi_j \quad (2c)$$

$$\dot{\zeta}_j = h\cdot\beta_j\cdot\psi_j - m_\zeta\cdot\zeta_j \quad (2d)$$

Where ***Q*** is the blood flow (perfusion), ***V*** is the volume and ***B*** is the nitrogen capacitance (different capacitance values were not calculated for helium, please refer to discussion). Notice that these three parameters are particular to a given compartment ***j*** and their values come from real physiological data [25,26]. The M-value ($M_{val}$) is also particular to the compartment ***j*** and its value comes from published tables. Not particular to a given compartment are the alveolar nitrogen pressure ($P_A$), the ambient pressure ($P_B$) and the blood capacitance for nitrogen ($B_S$). The values of $P_A$ and $P_B$ depend on the dive/decompression profile, while $B_S$ = 6.7x10$^{-10}$ mol m$^{-3}$ torr$^{-1}$ comes from physiological data. $\bar{\delta}$ is the non-linear operator that assumes the value 1 if the preceding term in brackets is positive and 0 if the preceding term in brackets

is negative. Both nitrogen pressure and bubble washout are given by the rate constant resulting from the ratio of blood perfusion to compartment volume.

Next, we describe the rate constants of the model, along with their respective units. For the sake of parametrization, each of these constants is assumed to be equal in all compartments.

• Rate constant $b$ (bubbles pressure$^{-1}$ time$^{-1}$) allows for bubble formation from or dissolution to the liquid phase depending on the difference between ambient and nitrogen pressure.

• Rate constant $z$ (bubble$^{-1}$ pressure$^{-1}$ time$^{-1}$) represents further nucleation sites due to inflammation.

• Rate constant $y$ ($\Psi$ pressure$^{-1}$ time$^{-1}$) relates the formation of proinflammatory factor $\Psi$ to nitrogen pressure above the supersaturation level of the compartment.

• Rate constant $f$ ($\Psi\,\zeta^{-1}$ time$^{-1}$) is the formation of factor $\Psi$ due to factor $\zeta$.

• Rate constant $g$ ($\Psi$ bubble$^{-1}$ time$^{-1}$) is the formation of factor $\Psi$ due to bubbles.

• Rate constant $h$ ($\zeta\,\Psi^{-1}$ bubble$^{-1}$ time$^{-1}$) is the formation of factor $\zeta$ due to the joint presence of bubbles and factor $\Psi$.

• Rate constants $m_\Psi$ and $m_\zeta$ (time$^{-1}$) are combined effects of physical washout and chemical/biological degradation of their respective factors.

• Rate constant $m_\beta$ is a value in the open interval $]0\,,1[$ representing the fraction of bubbles that are washed out from the compartment.

These rate constants have their values adjusted as described in a following section. Next, the compartments are described. All calculations were made assuming a rate of descent equal to 20 msw/minute and a rate of ascent equal to 9 msw/minute.

### 3.1. Compartments

Initially, the eight more relevant organic compartments were selected based on their masses and perfusion (bones were excluded from this selection). These organic compartments, their respective relative perfusion rate $\frac{Q_j}{V_j}$ (see above) and the combined washout rate $\frac{Q_j}{V_j}\frac{B_s}{B_j}$ in what would be an average adult man are listed in Table 5.

**Table 5: Compartments perfusion and washout rates**

| organ | $\frac{Q_j}{V_j}$ | $\frac{Q_j}{V_j}\frac{B_s}{B_j}$ |
|---|---|---|
| kidneys | $5.91 \times 10^{-2}$ | $4.74 \times 10^{-2}$ |
| liver | $1.23 \times 10^{-2}$ | $4.8 \times 10^{-3}$ |
| CNS | $8.05 \times 10^{-3}$ | $6.45 \times 10^{-3}$ |
| heart | $1.39 \times 10^{-3}$ | $1.11 \times 10^{-3}$ |
| skin | $1.52 \times 10^{-3}$ | $1.21 \times 10^{-3}$ |
| skeletal muscles | $5.75 \times 10^{-4}$ | $4.62 \times 10^{-4}$ |
| gastrointestinal tract | $1.94 \times 10^{-4}$ | $1.51 \times 10^{-4}$ |
| adipose tissues | $1.94 \times 10^{-4}$ | $3.76 \times 10^{-5}$ |

*Relative perfusion rate $\frac{Q_j}{V_j}$, $s^{-1}$ and combined washout rate $\frac{Q_j}{V_j}\frac{B_s}{B_j}$, $s^{-1}$ for the main body compartments of an average adult man*

The values of $a_j$ and $b_j$, used to calculate the maximum supersaturation values as defined in equation (1), were estimated through a simple interpolation of the values used in Bühlmann's ZHL 16 C for nitrogen, based on the compartment's calculated half-times. Next, body compartments that have approximately the same half-times were combined in a single compartment, creating a model of five compartments, as detailed in Table 6.

**Table 6. Compartment half-times**

| organs | compartment | half-time *(min)* |
|---|---|---|
| CNS, liver, kidneys | 1 | 2.4 |
| heart, skin | 2 | 9.5 |
| skeletal muscles | 3 | 25.1 |
| gastrointestinal tract | 4 | 74.3 |
| adipose tissue | 5 | 307.5 |

### 3.2. Rate constants

Inflammation is a rather intricate process that would render the model almost untreatable if one tries to insert a whole set of discrete real biological variables in it. Moreover, even the quantitative relationship among them (the rate constants in a model) would be missing in their majority, if not all. This is not to mention the absence of any quantitative measurement of the relationships between inflammation and inert gas bubbles. Therefore, the model comprises a series of parameters that follows from a simplified textual

**Table 7. Values of the rate constants in the model**

| rate constant | value |
|---|---|
| b | 2 |
| z | $10^{-4}$ |
| y | $10^{-1}$ |
| f | $10^{-5}$ |
| g | $10^{-6}$ |
| h | $10^{-8}$ |
| $m_\psi$ | $10^{-2}$ |
| $m_\zeta$ | $10^{-4}$ |
| $m_\beta$ | 0.5 |

description of an inflammatory process related to the lumped state variables ***Ψ*** and ***ζ*** (see above).

From data in another experimental protocol to a depth of 45 msw [23], we arbitrarily determined what would be considered a low-risk decompression profile in terms of bubble production and respective values of ***Ψ*** and ***ζ***. Simulating such a dive/decompression profile, we set the values of the biological parameters in order to: (1) let bubble formation rely mostly on the physical properties of the compartments; and (2) to prevent ongoing inflammation after the end of decompression. These values are presented in Table 7. This 45-msw dive and its decompression profile will be called "Standard" for the sake of comparisons and discussions in the following sections, as previously mentioned in the Materials and Methods section.

In order to check for the robustness of the results in face of the values of the rate constants, four tests were done. Firstly, the rate constant ***z*** was set to zero. This rate constant is the link between the inflammatory process and bubble formation, in a positive feedback loop (see equation 2b). Therefore, setting it to zero disconnects the physical and the biological processes (notice, however, that bubbles still produce inflammation – see rate constants ***g*** and ***h***, equations 2c and 2d).

The other three tests potentiate the inflammatory process, as described next. In a first test, the value of the parameter ***z***, which increases bubble formation due to the presence of the inflammatory factor ***ζ***, was increased 100-fold. In another, the limiting M-values of each compartment were decreased to one-half of their original estimated values. In the last one, the values of the rate constants ***z***, ***g*** and ***h*** were set to 20% higher than their respective original values.

## 4. RESULTS

### 4.1. Standard profile and changes in rate constants

Figure 2 shows the venous gas emboli predicted by the model for the standard profile (see Methods) with the values of the rate constants presented in Table 6. Figure 3 shows the dynamics of venous gas emboli when the rate constant ***z*** was set to zero. As it can be seen, the dynamics observed in Figure 3 are given basically by the physical properties of the compartments, and the inflammatory process does not interfere significantly with such a dynamic. In other words, for the standard profile, the bubble formation in the model does not depend on the biological process of inflammation, but is mainly driven by ambient pressure change, as intended (see "Rate constants" section). Figure 4 shows the simulations where the bubble formation was potentiated by the inflammatory process in the three settings described in the end of the preceding section.

### 4.2. Bubble grades observed by echocardiography

Mean bubble grades after each diving profile are shown in Tables 8 and 9. The complete dataset for each volunteer is given in the Appendix. Figure 5 shows the mean values along time for the two decompression profiles.

### 4.3. Comparison between experimental and model-generated venous bubble grades

Figure 6 shows the results of the simulations of the Adjusted ZHL and ZHL dive profiles. Venous gas emboli quantification in the model is arbitrary, and the quantification by echocardiographic EB scale is categorical. Therefore, a direct comparison in terms of "quantities" and their ratios is not as univocal as one might desire. The plots in Figure 6 indicate that the model captures some essential

**Figure 2**

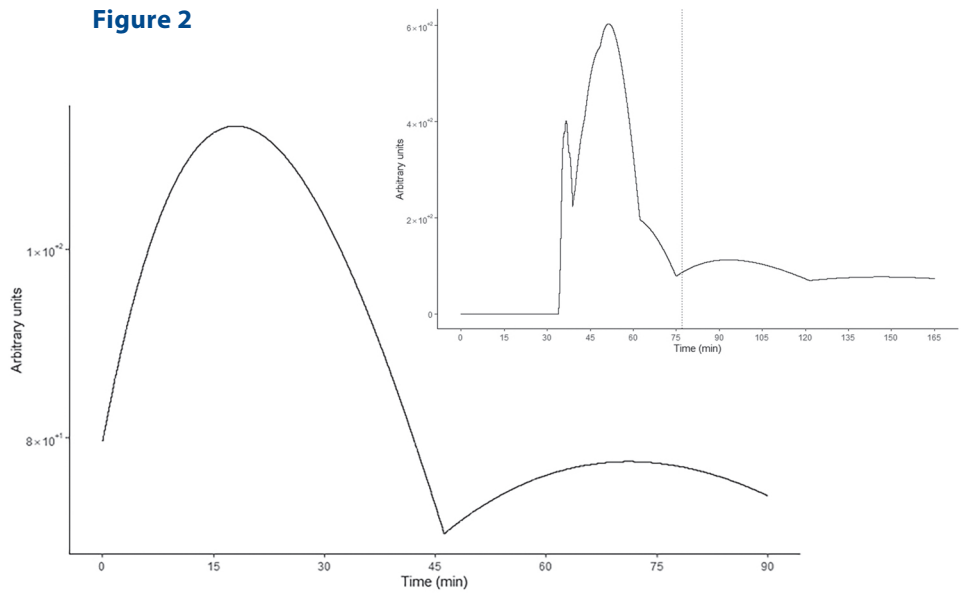


Venous gas emboli along time after emersion in the simulated standard profile with the basic set of rate constant values. Notice a second rise after 45 minutes of emersion, evidencing a non-simple decay of bubble dynamics after emersion. **Inset:** bubble formation along time from the beginning of the dive. The vertical dashed line indicates the moment of emersion. Notice that the majority of bubble formation occurs during the decompression phase, when ambient pressure is still higher than surface pressure.

**Figure 3**

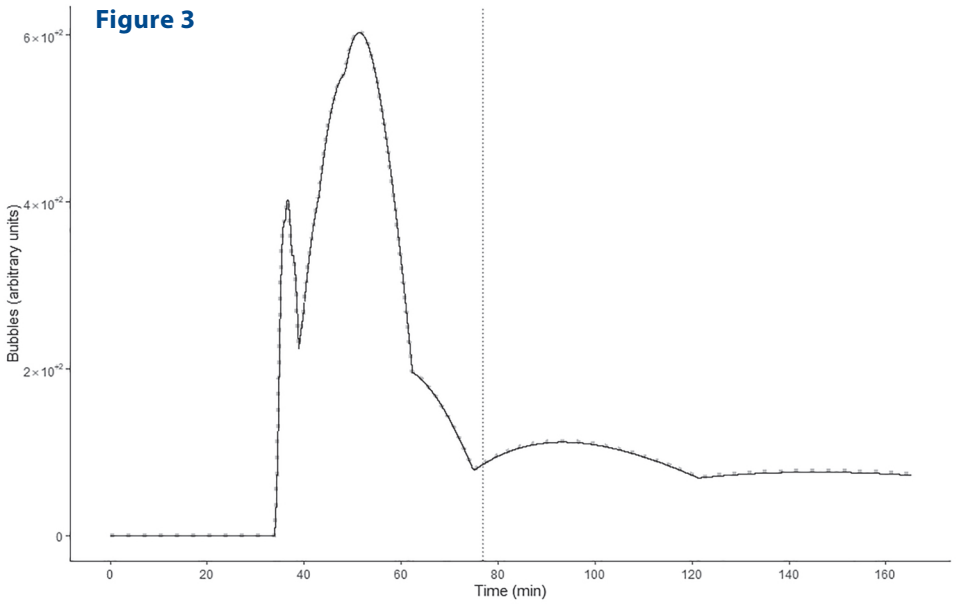


Venous gas emboli along time in the simulated standard profile with the basic set of rate constant values (black) and with the rate constant $z = 0$ (dotted line). Notice that the bubble formation profile is largely independent of the inflammatory process. **Vertical dotted line:** end of the dive.

features observed in Figure 5: the Adjusted ZHL profile produces fewer bubbles than the ZHL profile; both profiles have bubble observation peak sometime after emersion; bubble formation decays after 90 minutes from emersion. For a more detailed comparison, Figure 7 shows the simulation and the respective real data for each dive profile. In each panel, the simulated data were normalized to the maximum bubble grades.

It is worth mentioning that even though divers were using a breathing mix containing 35% helium during the experimental protocol, in the model, as a simplification, capacitance for helium for each compartment was not calculated, and it was assumed that only nitrogen would be present.

**Figure 4**

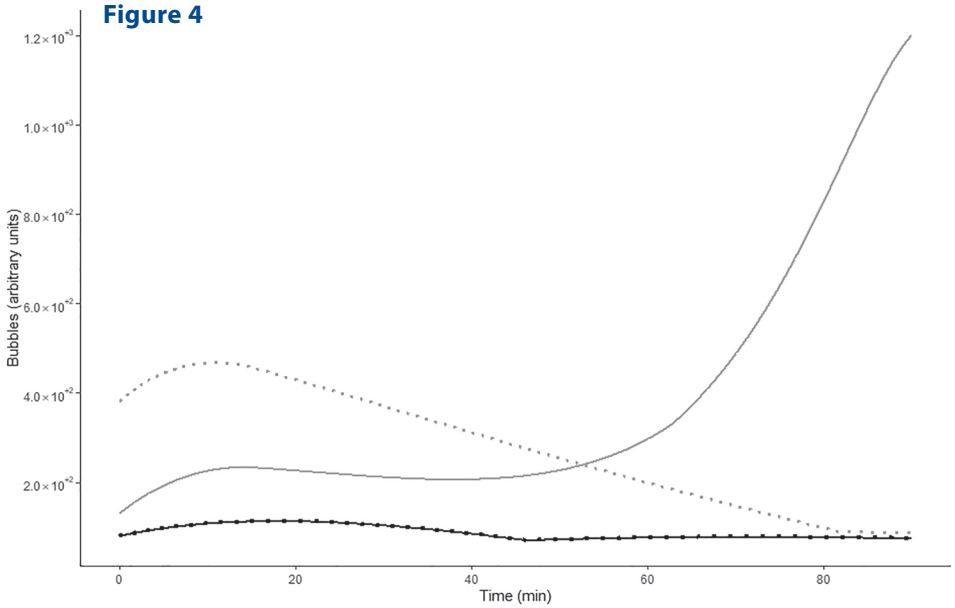


Venous gas emboli along time after emersion: potentiation of bubble formation by the inflammatory process.
**Grey solid line:** 100-fold increase in rate constant *z*.
**Grey dotted line:** decrease of M-values to one-half of their original values.
**Black dotted line:** simultaneous increase of 20% in rate constants *z*, *g* and *h*.
**Black solid line:** the standard profile, for comparison.

**Table 8. Mean bubble grade in the ZHL profile**

| | INTERVAL AFTER DIVE | | | | | | |
|---|---|---|---|---|---|---|---|
| | initial reading | 15 minutes | 30 minutes | 45 minutes | 60 minutes | 75 minutes | 90 minutes |
| mean | 2.2 | 2.55 | 2.88 | 2.35 | 2 | 1.75 | 1.65 |
| S.E. | 0.408 | 0.380 | 0.386 | 0.357 | 0.355 | 0.354 | 0.342 |

**Table 9. Bubble grade in the Adjusted-ZHL profile**

| | INTERVAL AFTER DIVE | | | | | | |
|---|---|---|---|---|---|---|---|
| | initial reading | 15 minutes | 30 minutes | 45 minutes | 60 minutes | 75 minutes | 90 minutes |
| mean | 1.8 | 2.15 | 2.56 | 2.15 | 1.9 | 1.6 | 1.35 |
| S.E. | 0.352 | 0.335 | 0.273 | 0.319 | 0.315 | 0.303 | 0.293 |

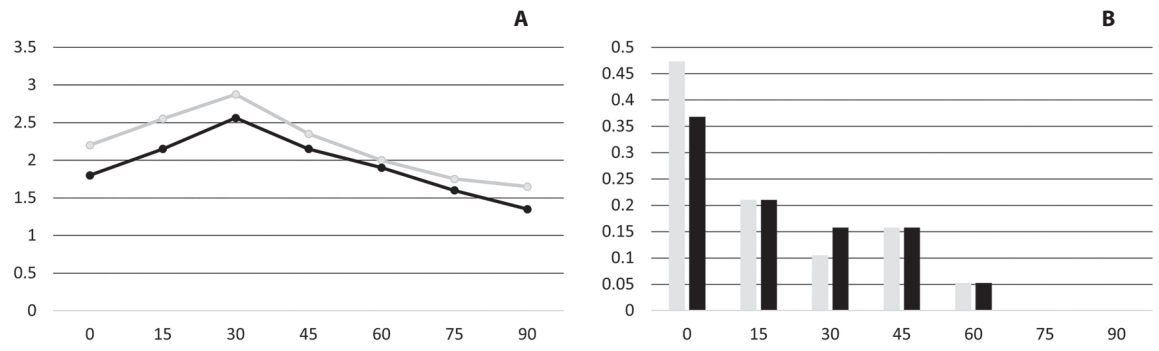


**Figure 5**

**(A)** Mean bubble grade along time for the two different decompression profiles.
**(B)** Fraction of individuals who peaked the bubble formation at a given time.
**Grey** ZHL; **Black** Adjusted-ZHL; time in minutes after emersion.

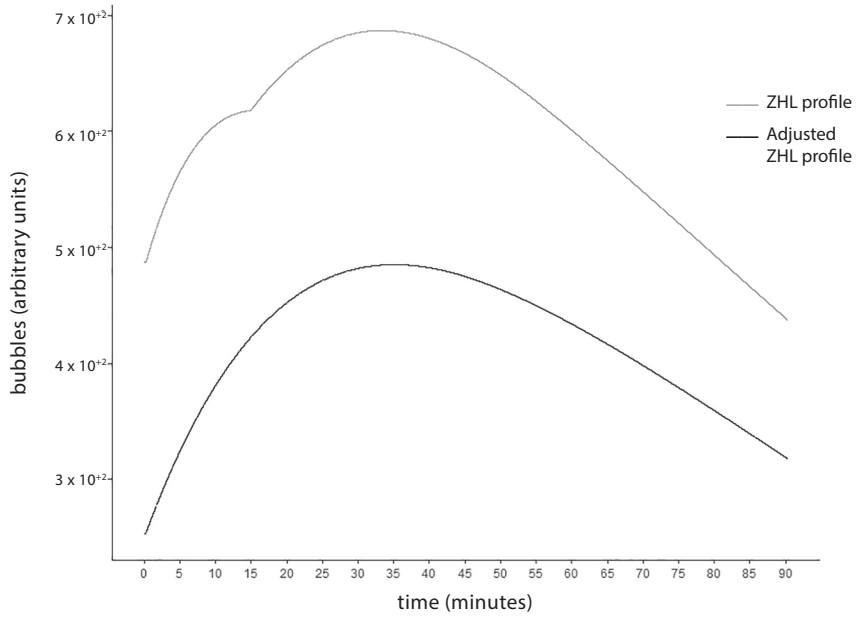


**Figure 6.**
Venous gas emboli in the simulations of the different profiles.

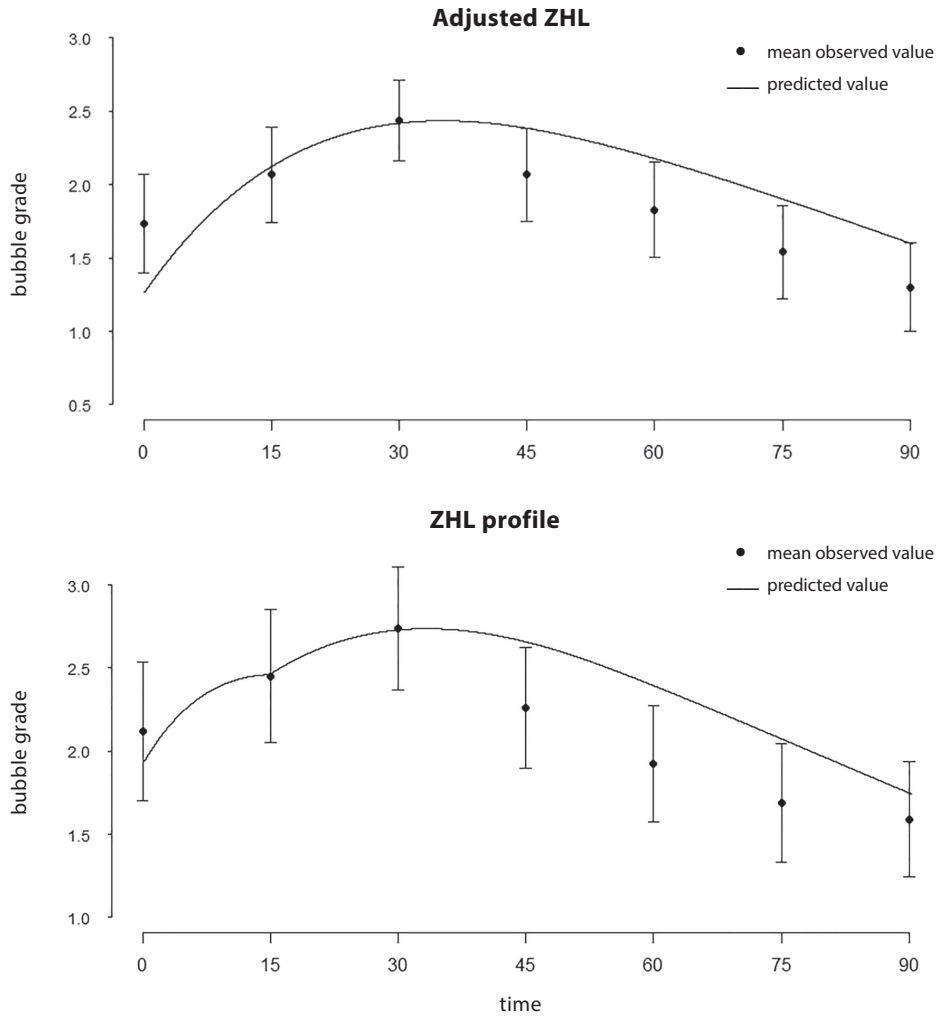


**Figure 7.**
Comparison of venous gas emboli in the simulated model with real bubble grade mean ± standard error for the period after emersion. Simulated results were normalized to the corresponding maximum bubble grades to fit the EB scale.

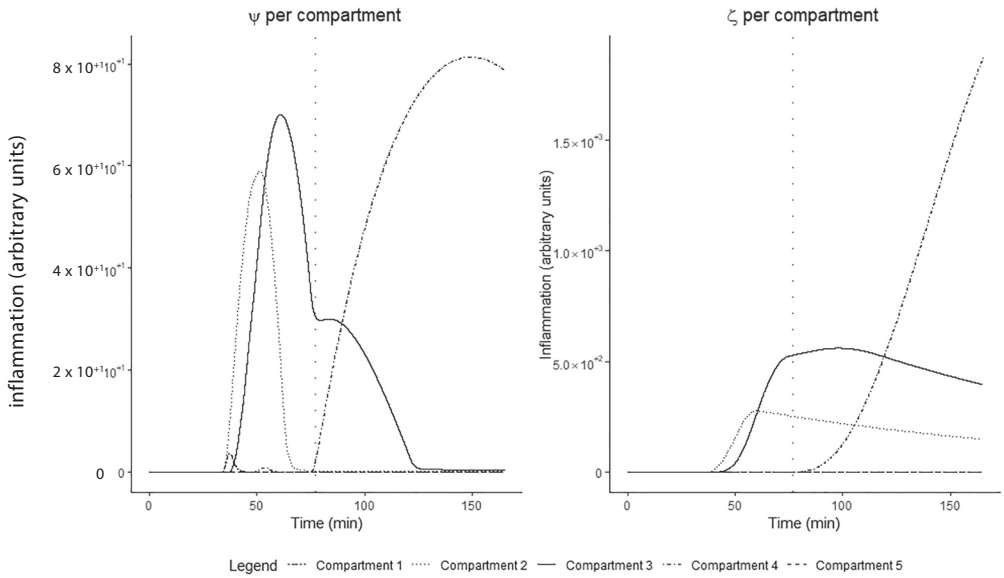


**Figure 8.**
Inflammatory state variables ***ψ*** and ***ζ*** in the diverse organic compartments along time of simulation for the standard dive profile.

This assumption, however, is consistent with results published by another study 27 and, although specific capacitance values for helium were not considered, the accuracy of our projected values seem satisfactory.

### 4.4. Inflammation

Figures 8, 9 and 10 show the dynamics of the state variables ψ and ζ in each organic compartment, according to Table 5, along all the simulation time for the standard, ZHL and Adjusted ZHL dive profiles. Based on the venous gas emboli dynamics presented in the preceding section, it would be expected the ZHL profile to have a higher level of the inflammatory state variables, followed by the Adjusted ZHL profile. Still based on estimated venous gas emboli, the standard profile would be expected to have the lower levels of inflammatory markers. In fact, this is what was observed. It is worth noting that for the three slower compartments part, if not all, of the important changes in inflammatory state variables occur after emersion.

In order to verify whether the increase in inflammation was caused only by increase in bubbles or if there was a mutual interaction among the state variables of the model, the rate constant ***z*** was set to zero (see section 4.1 and Figure 3), disconnecting increases in bubbles due to inflammation. The results are shown in Figure 11. As it can be seen, different from the results from simulations of the standard profile (section 4.1) where bubble production was mainly driven by changes in ambient pressure, inflammatory factors play a relevant role in bubble formation in these two profiles.

### 4.5. Extended bottom time and recompression

Figure 12 shows the simulation results for the standard profile with a 10-minute increase in bottom time (i.e., a total of 40 minutes at 45 msw), without a proportional increase in decompression time. Similarly to what was described in the preceding section, the levels of the inflammatory markers are dependent on the half-time

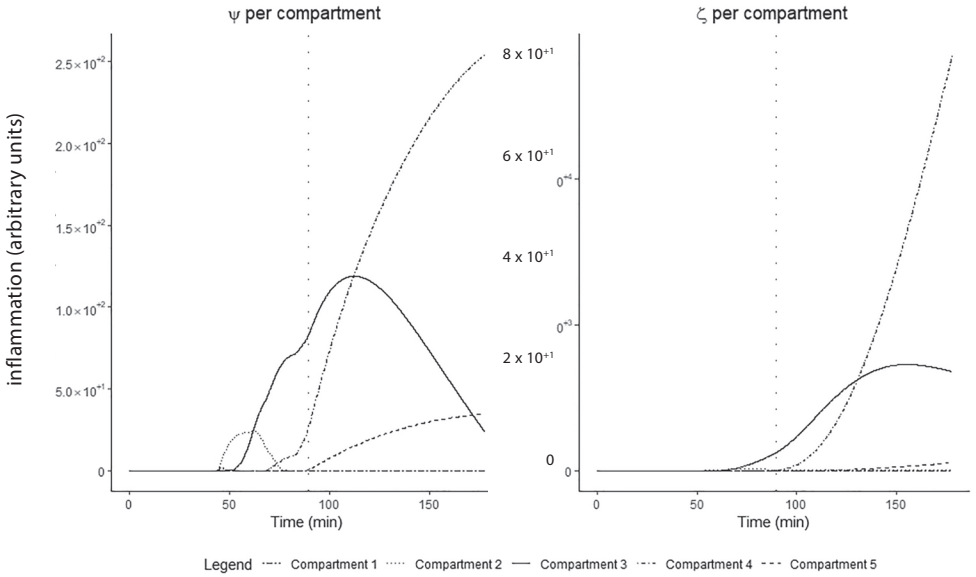


**Figure 9.**
Inflammatory state variables $\psi$ and $\zeta$ in the diverse organic compartments along time of simulation for the Adjusted ZHL dive profile.

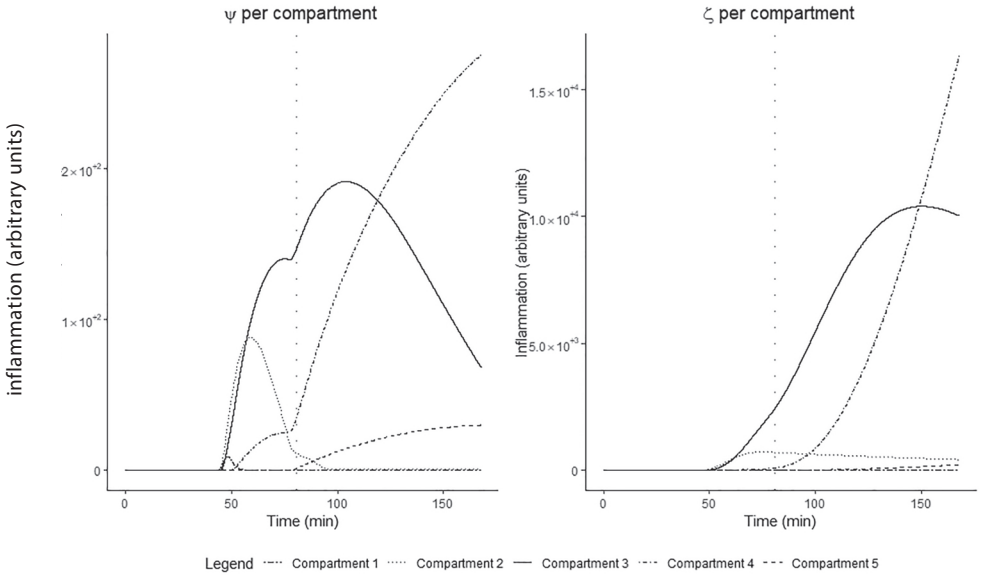


**Figure 10.**
Inflammatory state variables $\psi$ and $\zeta$ in the diverse organic compartments along time of simulation for the ZHL dive profile.

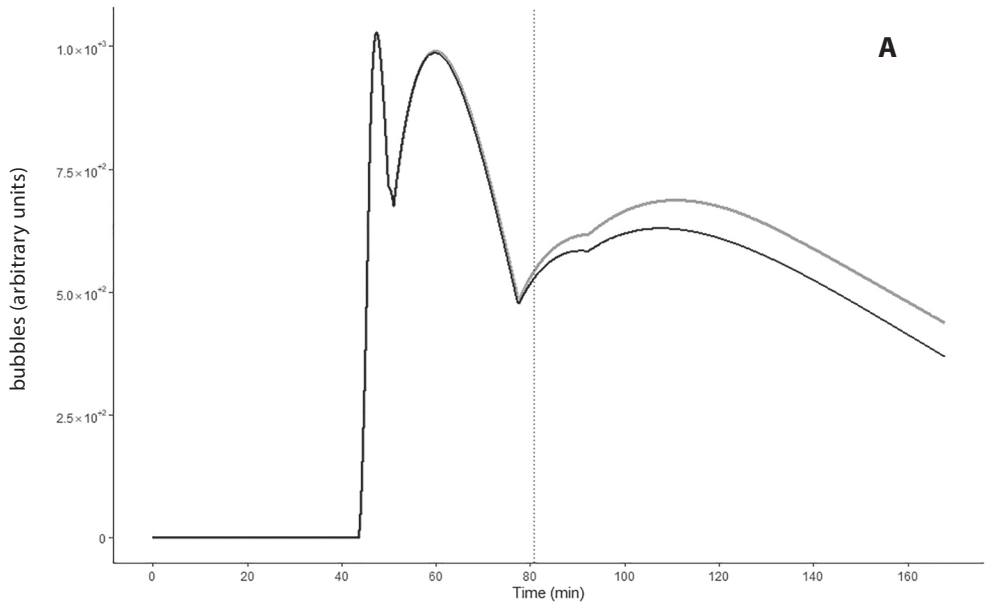


**Figure 11.**

Venous gas emboli along time in the ZHL (panel A) ▲ and Adjusted-ZHL (panel B) ▼ simulations.

**Black line:** rate constant $z = 0$; Grey line: $z = 10^{-4}$.

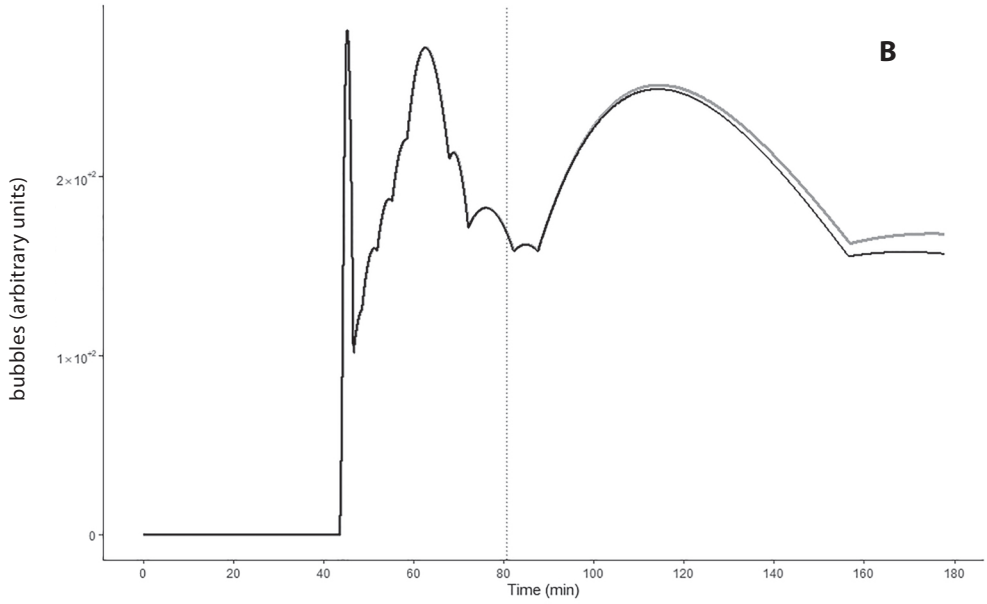

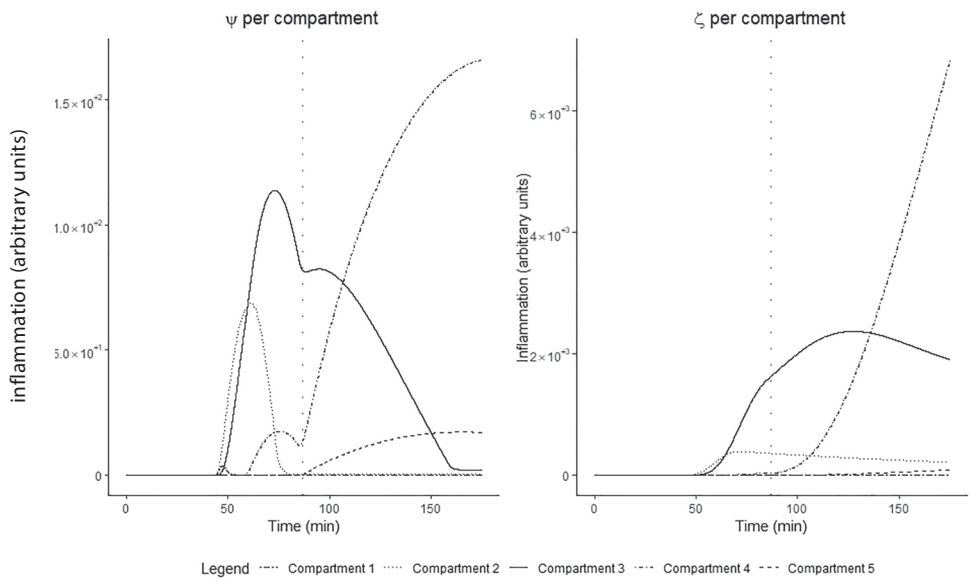


**Figure 12.**

Inflammatory state variables ***ψ*** and ***ζ*** in the diverse organic compartments along time of simulation for the standard profile with an increased bottom time of 10 minutes.

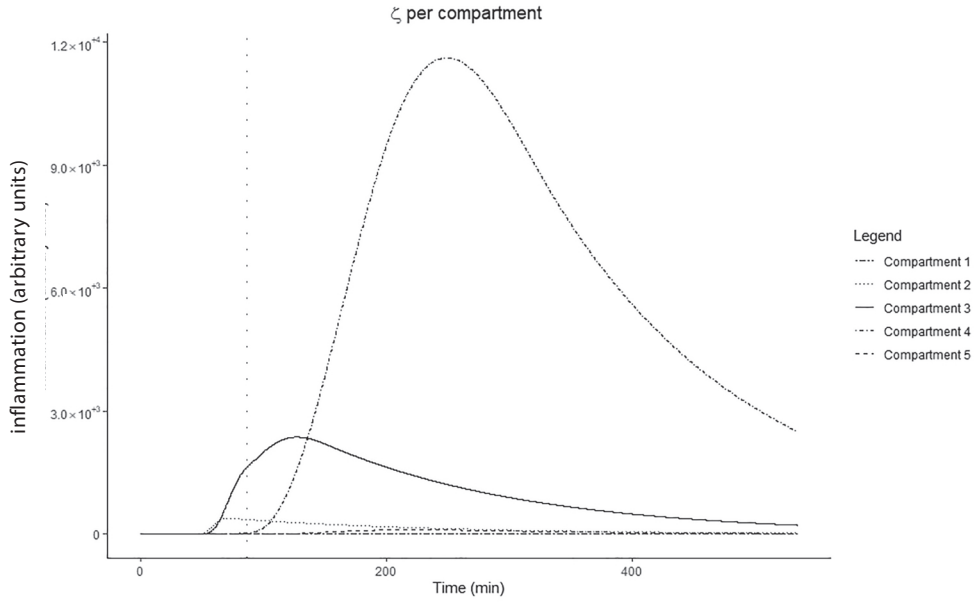


**Figure 13.**

Inflammation, given by ***ζ***, in the diverse organic compartments along time of simulation for the standard profile with an increased bottom time of 10 minutes, observed within an extended window of 500 minutes. Vertical dotted line: end of the dive.

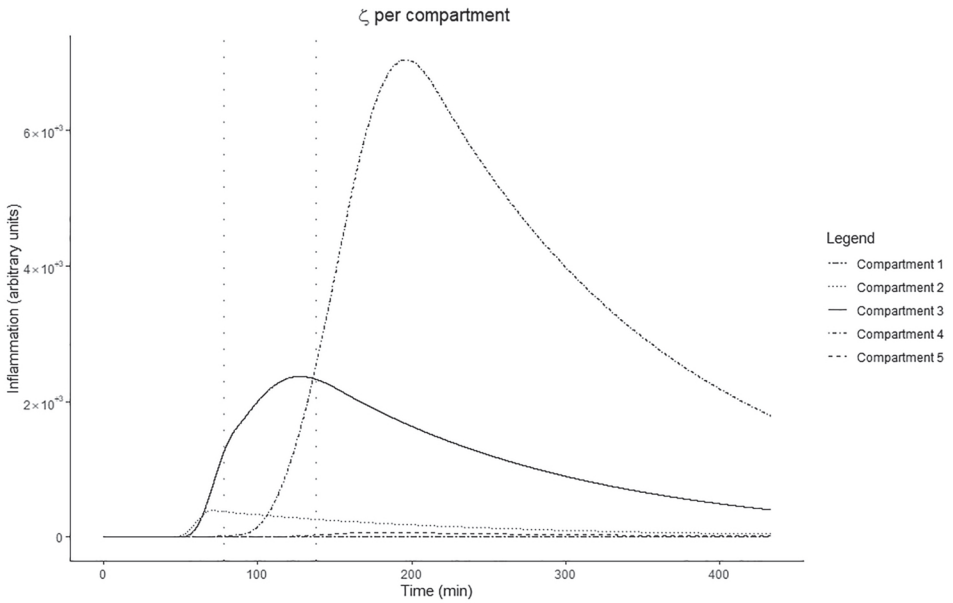


**Figure 14.**

Inflammation, given by ***ζ***, in the diverse organic compartments along time of simulation for the standard profile with an increased bottom time of 10 minutes followed by recompression, observed within an extended window of 500 minutes. First vertical dotted line from left to right: end of the dive; second vertical dotted line: begin of recompression.

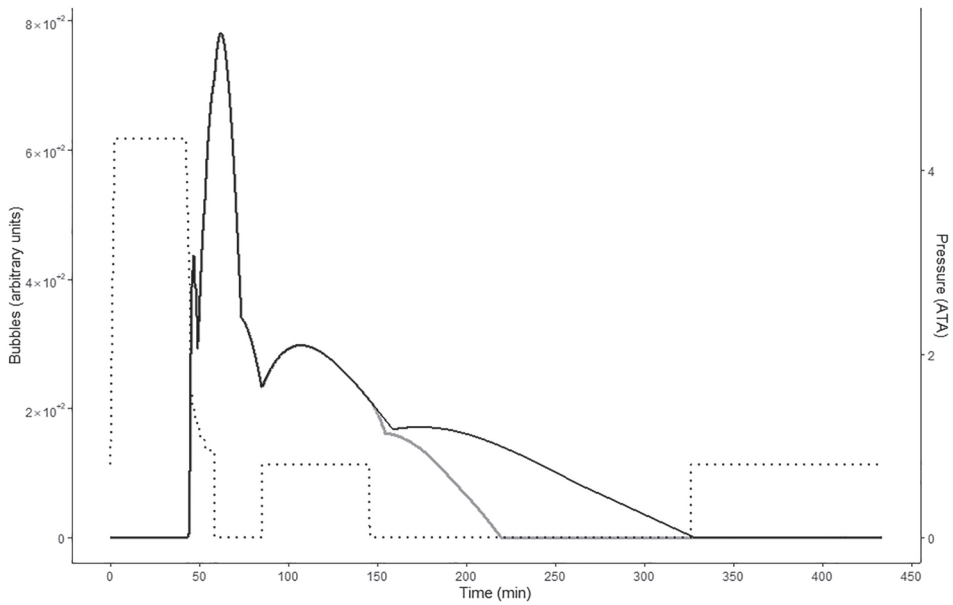


**Figure 15.**

Venous gas emboli along time of simulation for the standard profile with an increased bottom time of 10 minutes followed by recompression (in grey) and without recompression (in black), observed within an extended window of 500 minutes.
Dotted line represents the pressure of the inspired inert gas (right side scale).

of the compartments. Thus, while in the fastest compartment the standard profile presents a slightly higher level of inflammatory state variables, these levels change importantly as one goes to the slower compartments. It is interesting to note how the extension of bottom time, even for such a small amount as 10 minutes, would render a "safe" decompression profile into the "riskier" one (among the profiles simulated in the present study). This can be seen in the results of $\psi$ and $\zeta$ levels for compartments 3 and 4, which became much higher than those for the ZHL profile.

For the sake of completeness, Figure 13 illustrates the time profile of the state variable $\zeta$ for a total of 500 minutes. There one can see the peak of this variable in compartment 4 that occurs at around two and a half hours after the emersion and its subsequent slow decay.

Figure 14 illustrates the simulated effect of a recompression to a pressure of 162 kPa (6 msw) for 180 minutes, while breathing pure oxygen after an interval of 60 minutes at the surface (ambient pressure of 1 ATA). As can be observed, the levels of the inflammatory state variable $\zeta$ are reduced as a whole after recompression, with the peak in compartment 4 falling to about a half of its previous value and occurring 30 minutes earlier (Figure 13)

In Figure 15 the projected venous gas emboli for both profiles, with and without recompression, can be observed. The effects of recompression on venous gas emboli grades projected by the model accelerates the convergence to zero in more than 100 minutes in comparison with the scenario where no recompression is applied.

## 5. DISCUSSION

Modeling biological processes is difficult. Most of the time one can count only with very limited information regarding the variables at stake and how they relate to each other. As a consequence, most of the time one would end up with qualitative behaviors and not with closed quantitative answers even when physical events underlying the biological process are quite known [28,29]. In fact, the very modeling of decompression sickness is a vivid example of such a difficulty.

In this regard the present study addressed the putative interaction between bubble formation and inflammation during dive/decompression procedures by a non-extensive model of gas dynamics. On one hand, contrary to the proposal of Papadopoulou and colleagues [9] (Introduction), our model does not take into account detailed biophysical processes of bubble formation/dissolution. On the other hand, the model is grounded on realistic values of blood perfusion, tissue volume and nitrogen capacitance in the main organs of an average human being. In this sense it would be expected that the model could capture some average essential empirical findings in venous gas emboli, and in fact does (see section 4.3).

The nature of DCS – i.e., whether it should be classified as an inflammatory disease or as a consequence of mechanical damage caused by bubbles, or even as a combination of both – is far from a complete elucidation. The role of the inflammation associated with decompression has gained support in the past decade [30,31], even though the mechanism behind this interaction is presently unknown. Here, the interactions between bubbles and inflammation are given by three routes: bubbles inducing proinflammatory factors release; bubbles and proinflammatory factors promoting the increase in inflammatory factors; and inflammatory factors working as nucleation points for bubbles. These three routes are also grounded on experimental evidence [17-19, 31-36]. Thus, next, we briefly address each one of our results in order to contextualize the findings.

### The standard profile

The results shown in section 4.1 are important in order to verify that the values of the biological parameters do not add any significant number of bubbles in those simulations (Figures 2 and 3). Therefore, venous gas emboli along time follow a pattern that would be the same if only physical factors were taken into account. In this sense,

the model is quite similar to many other physical models of bubble formation in dive/decompression simulations.

Conversely, it is also shown that when increasing the connection strength between the processes, there is an increase in bubble formation, and such increase is related to which set of connections that was changed. M-values are related to ambient pressure and, thus, their effects in the system would be expected to be more pronounced during events where changes in pressure occur, while a positive feedback loop between bubbles and inflammation (the rate constant $z$) would be expected to have its effects in a later time. This is what the simulations show (see Figure 4).

Extended bottom time is expected to increase the potential for DCS if the decompression profile is not recalculated accordingly. This is in agreement with the estimated higher $\zeta$ values shown in Figures 12 and 13 in comparison with those displayed in Figure 8. As is widely known, recompression is a standard procedure to deal with manifest DCS. The present model suggests that this procedure abrogates bubble formation and further development of an ongoing inflammatory process (Figures 14 and 15). Therefore, if inflammation is a co-participant of DCS indeed, recompression might be effective in reversing this outcome due to a combined effect in both sides of the problem. Of course, there are probably other aspects of recompression not captured by the model, such as the potential anti-inflammatory effect of hyperbaric oxygen [37], and it is not the purpose of the present study to estimate all biochemical pathways related to DCS or recompression.

## Bubble grades and comparison to the model

When the model was simulated using the dive/decompression profiles of the experimental protocol, a relevant similarity between the echo-Doppler results and the simulated ones was obtained. The ZHL profile has more pronounced mean bubble grades along time than the Adjusted ZHL, even though the means at each time interval are not statistically significant. Both profiles have the peak in mean bubble grades around 30 minutes after emersion. The modeling shows the same time profile and relative amounts of venous gas emboli. Thus, in this sense, the model seems to capture how an average individual would respond to those dive/decompression profiles.

As cited before, Arieli and Marmur [10] define "bubblers" and "non-bubblers" in relation to unknown physiological variables leading to different amounts of gas emboli. Figure 5B shows another facet of the problem: Almost half of the volunteers have the peak (or the maximum) of bubble formation13 (or grade, according to the EB scale) at the moment of emersion, and a small fraction has their peak much later, around 60 minutes after emersion (see individual results in the Appendix). This means that not only amounts might vary among individuals, but the moment of their peak is a variable as well. In this sense, some rate constants of the present model might be adjusted in order to capture individual behaviors. For instance, the "at-emersion maximum" might be related to low M-values associated to low inflammation, resulting in an early peak without further progression. Presently, we only suggest this possibility, but our results give support to the prospect of setting the model to more individual responses.

## Inflammation

The main goal of the present study is to model a putative relationship between bubble formation and inflammation in dive/decompression procedures. In this sense, the model clearly captures such a putative interaction and shows that more aggressive profiles lead to more pronounced inflammatory processes (Figures 8, 9 and 10). In fact, the model shows that a relevant increase in bubble formation in these more daring profiles are due to the concomitant inflammatory process unleashed by the decompression (Figure 11). Additionally, as demonstrated in Figure 14, the model captures the effects of recompression on the dive-related inflammation due to interaction between bubble inflammatory state variables $\psi$ and $\zeta$.

The effect of the exposure to hyperbaric environments, even before decompression, has been shown to trigger platelet activation and platelet-derived MPs production [35], which could, in theory, create nucleation sites that later in the decompression would increase bubble observation. In this case, the inflammation and oxidative stress would precede the bubble formation. Or, as postulated by Imbert et al. [36], bubble production could be related to inherent unsaturation of tissues in a scenario where bubble formation would precede any inflammatory response. Both scenarios are compatible with the model described in the present study, and further research will be needed in order to fulfill our understanding of the many biochemical pathways involved in the development of DCS and its relationship to inflammation.

Another interesting point presented by the model is the contribution of different compartments to the overall process detected at the organismal level (for instance, bubble grades or platelet counts). The fast compartments, such as CNS, kidneys and heart, would have a low contribution to the overall process while the intermediary compartments, such as skeletal muscles and gastrointestinal tract, would be the main site of bubble/inflammation after the emersion. However, in dive profiles with exposures similar to those herein simulated, the very slow compartment of adipose tissue might end up unnoticed since gas dynamics is so lagging that the whole dive/decompression procedure occurs without any significant gas exchange in these tissues.

These results are obvious from the outset in the sense of gas dynamics, and previous models already have such in their core. What is new is that inflammation is shown to be potentially "exported" from one compartment to others and thus, even without arterial gas emboli, resonate the potential for DCS.

## 6. CONCLUSION

In the same spirit of the model advanced by Boudinet [38] our study intends to be a potential seed to a more comprehensive model of the development of gas emboli and the associated dysfunctions caused by decompression in order to forecast decompression sickness on an individual basis in the future.

## REFERENCES


1. Boycott AE, Damant GC, Haldane JS. The prevention of compressed-air Illness. J Hyg. Published online 1908: 342-443.

2. Strauss MB, Lu LQ, Miller SS. The Gradient Perfusion Model Part 1: Why and at what sites decompression sickness can occur. Undersea Hyperb Med. 2018;45(3):287-295.

3. Strauss MB, Lu LQ, Miller SS. The Gradient Perfusion Model Part 2: Substantiation of the GPM with clinical cases. Undersea Hyperb Med. 2018;45(3):297-305.

4. Lu LQ, Strauss MB, Miller SS. The Gradient Perfusion Model Part 3: An extraordinary case of decompression sickness. Undersea Hyperb Med. 2018;45(3):307-311.

5. Lewis GN. A mathematical model for decompression. Math Model. 1983;4(5):489-500. doi:10.1016/0270-0255(83)90052-0

6. Van Liew HD, Burkard ME. Density of decompression bubbles and competition for gas among bubbles, tissue, and blood. J Appl Physiol. 1993;75(5):2293-2301. doi: 10.1152/jappl.1993.75.5.2293

7. Chappell MA, Payne SJ. A physiological model of the release of gas bubbles from crevices under decompression. Respir Physiol Neurobiol. 2006;153(2):166-180. doi:10.1016/j.resp.2005.10.006

8. Gutvik CR, Brubakk AO. A dynamic two-phase model for vascular bubble formation during decompression of divers. IEEE Trans Biomed Eng. 2009;56(3):884-889. doi: 10.1109/TBME.2008.2005962

9. Papadopoulou V, Eckersley RJ, Balestra C, Karapantsios TD, Tang MX. A critical review of physiological bubble formation in hyperbaric decompression. Adv Colloid Interface Sci. 2013;191-192:22-30. doi:10.1016/j.cis.2013.02.002

10. Arieli R, Marmur A. A biophysical vascular bubble model for devising decompression procedures. Physiol Rep. 2017;5(6):1-11. doi:10.14814/phy2.13191

11. Doolette DJ. Gas micronuclei that underlie decompression bubbles and decompression sickness have not been identified. Diving Hyperb Med. 2019;49(1):64. doi:10.28920/dhm49.1.64

12. Doolette DJ. Venous gas emboli detected by two-dimensional echocardiography are an imperfect surrogate endpoint for decompression sickness. Diving Hyperb Med. 2016;46(1):4-10.

13. Papadopoulou V, Germonpré P, Cosgrove D, et al. Variability in circulating gas emboli after a same scuba diving exposure. Eur J Appl Physiol. 2018;118(6):1255-1264. doi:10.1007/s00421-018-3854-7

14. Cialoni D, Pieri M, Balestra C, Marroni A. Dive risk factors, Gas Bubble formation, and decompression illness in recreational SCUBA diving: Analysis of DAN Europe DSL data base. Front Psychol. 2017;8(SEP):1-11. doi:10.3389/fpsyg.2017.01587

15. Doolette DJ, Gault KA, Gutvik CR. Sample size requirement for comparison of decompression outcomes using ultrasonically detected venous gas emboli (VGE): Power calculations using Monte Carlo resampling from real data. Diving Hyperb Med. 2014;44(1):14-19.

16. Papadopoulou V, Germonpré P, Cosgrove D, et al. Variability in circulating gas emboli after a same scuba diving exposure. Eur J Appl Physiol. 2018;118(6):1255-1264. doi:10.1007/s00421-018-3854-7

17. Brett KD, Nugent NZ, Fraser NK, Bhopale VM, Yang M, Thom SR. Microparticle and interleukin-1β production with human simulated compressed air diving. Sci Rep. 2019;9(1):13320. doi:10.1038/s41598-019-49924-1

18. Thom SR, Bennett M, Banham ND, et al. Association of microparticles and neutrophil activation with decompression sickness. J Appl Physiol. 2015;119(5):427-434. doi:10.1152/japplphysiol.00380.2015

19. Thom SR, Milovanova TN, Bogush M, et al. Bubbles, microparticles, and neutrophil activation: Changes with exercise level and breathing gas during open-water SCUBA diving. J Appl Physiol. 2013;114(10):1396-1405. doi:10.1152/japplphysiol.00106.2013

20. Pontier JM, Jimenez C, Blatteau JE. Blood platelet count and bubble formation after a dive to 30 msw for 30 min. Aviat Sp Environ Med. 2008;79(12):1096-1099. doi:10.3357/ASEM.2352.2008

21. Pontier JM, Vallée N, Bourdon L. Bubble-induced platelet aggregation in a rat model of decompression sickness. J Appl Physiol. 2009;107(6):1825-1829. doi:10.1152/japplphysiol.91644.2008

22. Bühlman A. Decompression, Decompression Sickness. Springer Verlag Berliin Heidelberg; 1984. doi:10.1007/978-3-662-02409-6

23. Schirato SR, El-dash I, El-dash V, Natali JE, Starzynski PN, Chaui-berlinck JG. Heart rate variability changes as an indicator of decompression-related physiological stress. Undersea Hyperb Med. 2018;Mar-Apr 20:173-182.

24. Eftedal O, Brubakk AO. Detecting intravascular gas bubbles in ultrasonic images. Med Biol Eng Comput. 1993;31(November):627-633. doi:10.1007/ BF02441812

25. Valentin J. Basic anatomical and physiological data for use in radiological protection: reference values. Ann ICRP. 2002;32(3-4):1-277. doi:10.1016/S0146-6453(03)00002-2

26. Altman PL, Dittmer DS. Biological Handbooks: Respiration and Circulation. FASEB; 1971.

27. Doolette DJ, Upton RN, Grant C. Altering blood flow does not reveal differences between nitrogen and helium kinetics in brain or in skeletal miracle in sheep. J Appl Physiol (1985). 2015. doi:10.1152/japplphysiol.00944.2014

28. Chaui-Berlinck JG, Navas CA, Monteiro LHA, Bicudo JEPW. Temperature effects on a whole metabolic reaction cannot be inferred from its components. Proc Biol Sci. 2004;271(1546):1415-1419. doi:10.1098/rspb.2004.2727

29. Chaui-Berlinck JG, Navas CA, Monteiro LHA, Bicudo JEPW. Control of metabolic rate is a hidden variable in the allometric scaling of homeotherms. J Exp Biol. 2005;208(Pt 9):1709-1716. doi:10.1242/jeb.01421

30. Brubakk AO, Møllerløkken A. The role of intra-vascular bubbles and the vascular endothelium in decompression sickness. Diving Hyperb Med. 2009 Sep;39(3):162-169.

31. Madden LA, Laden G. Gas bubbles may not be the underlying cause of decompression illness - The at-depth endothelial dysfunction hypothesis. Med Hypotheses. 2009;72(4):389-392. doi:10.1016/j.mehy.2008.11.022

32. Zhang K, Wang M, Wang H, Liu Y, Buzzacott P, Xu W. Time course of endothelial dysfunction induced by decompression bubbles in rats. Front Physiol. 2017;8(MAR):1-9. doi:10.3389/fphys.2017.00181

33. Thom SR, Bhopale VM, Yang M. Neutrophils generate microparticles during exposure to inert gases due to cytoskeletal oxidative stress. J Biol Chem. 2014;289(27):18831-18845. doi:10.1074/jbc.M113.543702

34. Thom SR, Milovanova TN, Bogush M, et al. Microparticle production, neutrophil activation, and intravascular bubbles following open-water SCUBA diving. J Appl Physiol. 2012;112(8):1268-1278. doi:10.1152/japplphysiol.01305.2011

35. Bhullar J, Bhopale VM, Yang M, Sethuraman K, Thom SR. Microparticle formation by platelets exposed to high gas pressures – An oxidative stress response. Free Radic Biol Med. 2016;101(October):154-162. doi:10.1016/j.freeradbiomed.2016.10.010

36. Imbert J-P, Egi SM, Germonpré P, Balestra C. Static metabolic bubbles as precursors of vascular gas emboli during divers' decompression: a hypothesis explaining bubbling variability.. Front Physiol. 2019;10(July):1-12. doi:10.3389/fphys.2019.00807

37. Bitterman H, Muth CM. Hyperbaric oxygen in systemic inflammatory response. Intensive Care Med. 2004;30(6): 1011-1013. doi:10.1007/s00134-004-2211-y

38. Boudinet P. A new dynamical theory of decompression. Adv Res. 2018;17(1):1-20. doi:10.9734/air/2018/44062